

Distillation-free Scaling of Large SSMs for Images and Videos

Hamid Suleman^{*1,2}, Syed Talal Wasim^{*1,2}, Muzammal Naseer³, Juergen Gall^{1,2}

¹University of Bonn, Germany

²Lamarr Institute for Machine Learning and Artificial Intelligence, Germany

³Center of Secure Cyber-Physical Security Systems, Khalifa University, Abu Dhabi, United Arab Emirates
hsuleman@uni-bonn.de, swasim@uni-bonn.de, muzammal.naseer@ku.ac.ae, gall@iai.uni-bonn.de

*Equal Contribution

Abstract

State-space models (SSMs), exemplified by S4, have introduced a novel context modeling method by integrating state-space techniques into deep learning. However, they struggle with global context modeling due to their data-independent matrices. The Mamba model addressed this with data-dependent variants via the S6 selective-scan algorithm, enhancing context modeling, especially for long sequences. However, Mamba-based architectures are difficult to scale with respect to the number of parameters, which is a major limitation for vision applications. This paper addresses the scalability issue of large SSMs for image classification and action recognition without requiring additional techniques like knowledge distillation. We analyze the distinct characteristics of Mamba-based and Attention-based models, proposing a Mamba-Attention interleaved architecture that enhances scalability, robustness, and performance. We demonstrate that the stable and efficient interleaved architecture resolves the scalability issue of Mamba-based architectures for images and videos and increases robustness to common artifacts like JPEG compression. Our thorough evaluation on the ImageNet-1K, Kinetics-400 and Something-Something-v2 benchmarks demonstrates that our approach improves the accuracy of state-of-the-art Mamba-based architectures by up to +1.7.

1 Introduction

Various networks have been proposed for both image and video recognition in recent years. These include convolutional neural networks (Krizhevsky, Sutskever, and Hinton 2012; He et al. 2016; Carreira and Zisserman 2017; Feichtenhofer et al. 2019), vision Transformers (Dosovitskiy et al. 2021; Arnab et al. 2021), and networks using focal modulation (Yang et al. 2022; Wasim et al. 2023). The Attention-based Transformer models have dominated both image and video recognition, either as pure Attention-based models (Liu et al. 2021, 2022c; Arnab et al. 2021; Bertasius, Wang, and Torresani 2021; Yan et al. 2022) or as hybrid models (Li et al. 2022a; Fan et al. 2021; Li et al. 2022b).

Recently, State-Space Models (SSMs) such as S4 (Gu, Goel, and Ré 2022) have gained popularity as a new context modeling method. They recurrently model context and

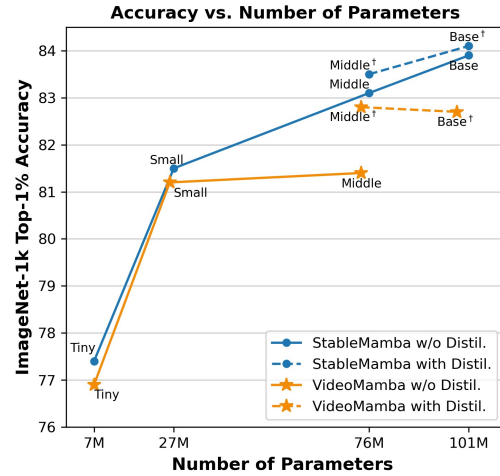


Figure 1: **Performance comparison with VideoMamba:** We compare the performance of our model with VideoMamba (Li et al. 2024), both with and without distillation, on IN1K (Deng et al. 2009).

bring well-established techniques from state-space modeling to deep large models. However, S4 encountered a problem in terms of modeling global context due to the data-independent nature of the input, state-transition, and output matrices. To mitigate this issue, the Mamba (Gu and Dao 2023) model introduced the S6 selective-scan algorithm, which uses data-dependent variants of the input and output matrices. This improves the context modeling capabilities, particularly on long sequences, and the approach has been adapted to image tasks (Zhu et al. 2024; Liu et al. 2024b) and in the recent work VideoMamba (Li et al. 2024) to the video domain.

In this work, we investigate the property of vision SSMs, where we focus on VideoMamba (Li et al. 2024) since it is the largest vision SSM architecture and the only that can be applied to videos, and make two key observations. First, VideoMamba does not scale well with the amount of parameters as plotted in Figure 1. While the accuracy substantially increases as the number of parameters is increased from 7M (tiny) to 25M (small) parameters, the accuracy only slightly increases if the parameters are increased further to

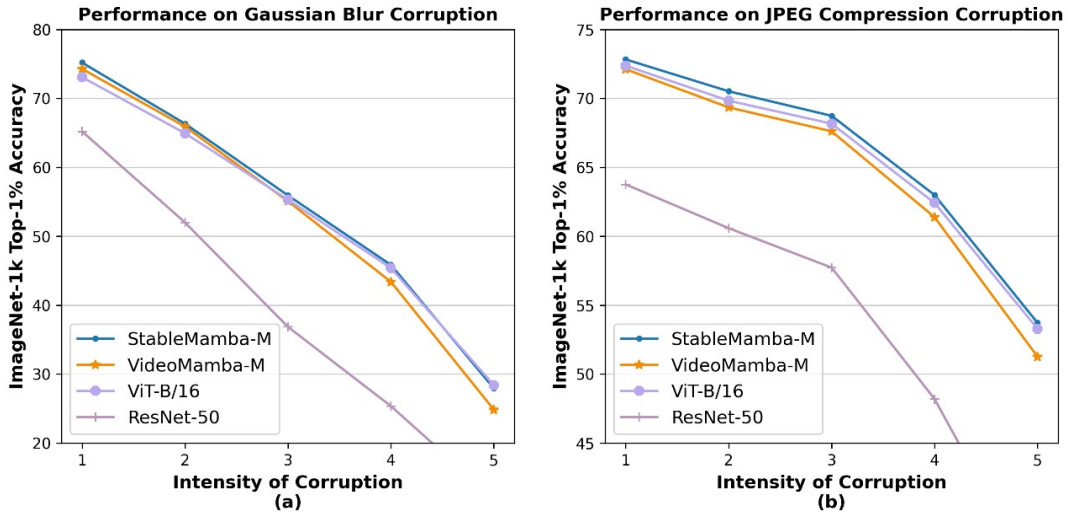


Figure 2: (a) Performance comparison of different networks on Gaussian blur corruption. (b) Performance comparison of different networks on JPEG compression corruption.

75M (middle) parameters. To mitigate this issue, Li et al. (2024) proposed to train first a small model and then use the small model as the teacher for training a larger model using distillation. While distillation improves the accuracy of the middle-sized model, it does not solve the underlying problem. Increasing the parameters further to 98M (base) parameters again does not improve the results. The second observation is the higher sensitiveness of the Mamba-based network to common corruptions and perturbations like image blur or JPEG compression in comparison to vision Transformers as shown in Figure 2. Both observations are major limitations for practical applications. We therefore propose a simple yet efficient Mamba-Attention interleaved architecture, termed StableMamba, that resolves both issues. It improves the robustness to common corruptions and perturbations during inference (Hendrycks and Dietterich 2019) as shown in Figure 2 and mitigates the scalability issue without the need of cumbersome workarounds like distillation as shown in Figure 1. In summary, the main contributions of this paper are:

- We analyze the largest Mamba architecture for images and video and present a simple yet efficient Mamba-Attention interleaved architecture.
- We show that our approach resolves the scalability issue and increases the robustness to various common corruptions (Hendrycks and Dietterich 2019).
- We report improved performance for comparable methods for image classification on ImageNet-1K (Deng et al. 2009) and for action recognition on Kinetics-400 (Kay et al. 2017) and Something-Something-v2 (Goyal et al. 2017).

2 Related Work

Image and Video Recognition: In the last decade, Convolutional Neural Networks (CNNs) have been the primary

choice for computer vision tasks. Starting with the introduction of AlexNet (Krizhevsky, Sutskever, and Hinton 2012), the field has seen rapid advancements with notable architectures such as VGG (Simonyan and Zisserman 2015), Inception (Szegedy et al. 2015), ResNet (He et al. 2016), MobileNet (Howard et al. 2017), and EfficientNet (Tan and Le 2019) achieving improved performance on ImageNet (Deng et al. 2009). Recently, ConvNeXt variants (Liu et al. 2022a; Woo et al. 2023) and FocalNets (Yang et al. 2022) have updated traditional 2D ConvNets with modern design elements and training techniques, achieving performance comparable to state-of-the-art models. At the same time, the Vision Transformer (ViT) (Dosovitskiy et al. 2021), inspired by the Transformer (Vaswani et al. 2017) for natural language processing, and its variants such as DeiT (Touvron et al. 2021a), Swin Transformer (Liu et al. 2021), and Swin Transformer V2 (Liu et al. 2022c) have achieved very good results for image classification.

For Video Recognition, early methods were feature-based (Klaser, Marszałek, and Schmid 2008; Laptev and Lindeberg 2003; Wang et al. 2013). Later, the success of 2D CNNs (Krizhevsky, Sutskever, and Hinton 2012; Simonyan and Zisserman 2015; He et al. 2016; Tan and Le 2019) on ImageNet (Deng et al. 2009) lead to their application to video recognition (Karpathy et al. 2014; Ng et al. 2015; Simonyan and Zisserman 2014). However, these methods lacked temporal modeling capabilities. The release of large-scale datasets such as Kinetics (Kay et al. 2017) prompted 3D CNN based methods (Carreira and Zisserman 2017; Feichtenhofer, Pinz, and Wildes 2016; Tran et al. 2015). Since these were computationally expensive, various methods were proposed to mitigate the issue (Feichtenhofer 2020; Sun et al. 2015; Szegedy et al. 2016; Tran et al. 2018; Xie et al. 2018; Li et al. 2020b; Lin, Gan, and Han 2019; Qiu et al. 2019; Feichtenhofer et al. 2019; Duan et al. 2020; Li et al. 2020a; Wang et al. 2021). When the

ViT (Dosovitskiy et al. 2021) architecture became popular in image recognition, it seamlessly made its way into the video domain. Initial methods used Self-Attention in combination with CNNs (Wang et al. 2018, 2020b; Kondratyuk et al. 2021) while later works (Liu et al. 2022b; Arnab et al. 2021; Bertasius, Wang, and Torresani 2021; Yan et al. 2022; Zhang et al. 2021; Patrick et al. 2021; Fan et al. 2021; Li et al. 2022b; Patrick et al. 2021; Sharir, Noy, and Zelnik-Manor 2021) introduced pure Transformer based architectures. More recently, Video-FocalNets (Wasim et al. 2023) proposed a Focal Modulation (Yang et al. 2022) extension for videos, while Uniformer (Li et al. 2022a) proposed an efficient hybrid architecture for video recognition. Very recently, a key development in this area came with FlashAttention (Dao et al. 2022; Dao 2023), which presents a hardware-aware implementation of the Attention algorithm, mitigating the quadratic compute complexity issue of Attention-based models.

State Space Models: Recently, State-Space Models (SSMs), such as the Structured State-Space Model (S4 (Gu, Goel, and Ré 2022)), have been presented as an alternative to Self-Attention (Vaswani et al. 2017) for efficient modeling of long sequences with linear complexity. Various variants building on the S4 architecture have also been proposed, including S5 (Smith, Warrington, and Linderman 2023), H3 (Fu et al. 2023), and GSS (Mehta et al. 2022). However, the original S4 (Gu, Goel, and Ré 2022) and its variants had a weakness compared to Self-Attention, mainly because they did not have any input dependencies. To mitigate this, Mamba (Gu and Dao 2023) proposed an input-dependent state-space model alongside an efficient hardware-optimized parallel selective scan mechanism (S6). Various works have been proposed in computer vision applying Mamba to different downstream domains. Two variants were initially proposed for image classification: Vim (Zhu et al. 2024) and VMamba (Liu et al. 2024b). Vim proposed an isotropic architecture with a bi-directional scanning variant of Mamba (Gu and Dao 2023) for effectively scanning the image token sequence. In contrast, VMamba (Liu et al. 2024b) proposed a hierarchical architecture with a four-directional scan across all four spatial dimensions. Subsequently, other variants such as LocalVMamba (Huang et al. 2024) had a Swin (Liu et al. 2021) style windowed scan while EfficientVMamba (Pei, Huang, and Xu 2024) proposed an atrous-selective scan to improve efficiency. Furthermore, Mamba was also used in various applications in video understanding (Yang, Xing, and Zhu 2024; Li et al. 2024; Chen et al. 2024), image segmentation (Liu et al. 2024a; Ma, Li, and Wang 2024; Ruan and Xiang 2024; Gong et al. 2024), and various other tasks (Guo, Wang, and Meng 2024; He et al. 2024; Wang et al. 2024; Guo et al. 2024; Liang et al. 2024). SiMBA (Patro and Agneeswaran 2024) uses the Fourier transform with nonlinearities to model eigenvalues as negative real numbers in an attempt to improve the training. Similar methods have also been proposed for CNNs (Wang et al. 2020a) and Transformer (Xiao et al. 2021; Touvron et al. 2021a,b). A concurrent work to ours, VideoMamba (Li et al. 2024), proposes to use a distillation-based objective to stabilize the training

of larger models. However, we show that a simple interleaving of Self-Attention layers within a Mamba-based model is enough to stabilize training for image and action recognition applications and improve robustness against high frequencies in the input.

3 Limitations of Mamba-based Networks for Visual Recognition

Although Mamba-based networks have shown state-of-the-art performance for image classification (Li et al. 2024; Zhu et al. 2024) and action recognition (Li et al. 2024), their training is unstable, which limits the scalability of these architectures. For instance, VideoMamba (Li et al. 2024) uses a distillation technique to improve training stability and performance. Since the proposed self-distillation technique requires training smaller models first, it is a cumbersome approach that increases the training cost.

Before we propose our solution to the scalability problem in Section 4, we analyze the behavior of pure Mamba-based visual architectures in more detail. We focus on VideoMamba (Li et al. 2024) since it is the largest architecture and the only one that can be applied to video data. VideoMamba trains its tiny and small models with 7M and 25M parameters, respectively, in a conventional setting. However, distillation is used to train it as soon as the parameters are scaled up to the middle model (75M parameters) and base model (98M parameters). The method uses the smaller model as the teacher for the larger middle and base models. This is a departure from the general knowledge distillation where a larger complex model is distilled into a smaller student model (Gou et al. 2020). This reversal suggests that the purpose of distillation is not merely to transfer knowledge from a simpler model to a complex one but to stabilize the learning process of the middle and base models. As shown in Figure 1, the architecture cannot be scaled beyond 25M parameters without distillation, i.e., the accuracy does not increase further. While distillation improves the accuracy, it does not address the scaling issue since the base model is not better than the middle model. To better understand the impact of distillation on the training, we trained VideoMamba’s middle variant with and without distillation. The training curves shown in Figure 3 indicate the presence of instabilities without distillation.

Furthermore, in Figure 2, we compare the behavior of VideoMamba (Li et al. 2024) with ViT-B\16 (Dosovitskiy et al. 2021) under an increasing amount of Gaussian blurring in the input image during inference. For this, we use the images from the ImageNet-C (Hendrycks and Dietterich 2019) benchmark, which evaluates the robustness of networks to common corruptions like Gaussian blur. As shown in Figure 2(a), VideoMamba (Li et al. 2024) suffers more than the vision Transformer from high intensities of Gaussian blurring. The better robustness of ViT-B\16 can be explained by the fact that Transformers tend to focus on lower frequencies in the input image (Naseer et al. 2021). This observation is further supported by another experiment that examines the behavior of networks under JPEG compression corruption. JPEG compression primarily removes high frequencies as

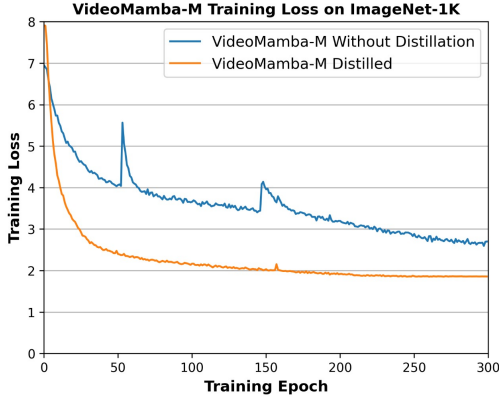


Figure 3: Loss curves obtained from training VideoMamba with and without distillation.

the compression rate increases, although it also introduces tertiary compression-related artifacts as well. The removal of higher frequencies remains the dominant effect. Figure 2 (b) shows that the VideoMamba is less robust to corruptions of higher frequencies, and addressing this challenge is an important contribution of this paper.

The above-mentioned observations provide enough evidence that it is difficult to scale Mamba models. Using distillation with a smaller model is a workaround to address training instabilities for larger models since it penalizes the larger model for deviating from the smaller one and thus acts as a regularization constraint, but it does not resolve the scalability issue. Furthermore, they are less robust to common image corruptions than vision Transformers. We thus propose an efficient distillation-free solution that mitigates the scalability issue, including training stability issues for large models, and improves the robustness to common image corruptions. Our solution is motivated by the fact that vision Transformers suffer less from these issues and we hypothesize that adding attention blocks to pure Mamba-based visual architectures resolves these issues. We evaluate the effectiveness of this hypothesis in the subsequent sections.

4 StableMamba for Image Classification and Action Recognition

Before discussing the StableMamba architecture in Section 4.2, we briefly introduce state-space models in general.

4.1 State-Space Models

State-space models (SSMs) are inspired by continuous systems in which an input signal $u(t)$ is mapped to a latent state $h(t)$ before being mapped to an output signal $y(t)$. Concretely, a linear ordinary differential equation describes the SSM model:

$$\begin{aligned} h'(t) &= \mathbf{A}h(t) + \mathbf{B}u(t) \\ y(t) &= \mathbf{C}h(t) \end{aligned} \quad (1)$$

where $h(t)$ is the hidden state, $h'(t)$ is the first derivative, $u(t)$ is the input, and $y(t)$ is the output. \mathbf{A} is the evolution

matrix, and \mathbf{B} and \mathbf{C} are the projection matrices of the system.

Discretization of State-Space Models: As mentioned before, eq. (1) is valid for continuous time systems. To apply eq. (1) on a discretized input sequence (u_0, u_1, u_2, \dots) instead of a continuous function $u(t)$, eq. (1) must be discretized using a step size Δ which describes the input time-step resolution. The standard discretization that follows Mamba (Gu and Dao 2023) is the Zero-Order Hold (ZOH) discretization:

$$\begin{aligned} \bar{\mathbf{A}} &= \exp(\mathbf{A}) \\ \bar{\mathbf{B}} &= (\mathbf{A})^{-1}(\exp(\mathbf{A}) - \mathbf{I}) \cdot \mathbf{B} \\ h_t &= \bar{\mathbf{A}}h_{t-1} + \bar{\mathbf{B}}u_t \\ y_t &= \mathbf{C}h_t. \end{aligned} \quad (2)$$

The difference between S4 (Gu, Goel, and Ré 2022) and Mamba (Gu and Dao 2023) is the selective scan mechanism that conditions the parameters of \mathbf{A} , \mathbf{B} , and \mathbf{C} .

4.2 StableMamba

VideoMamba (Li et al. 2024) uses bi-directional Mamba layers introduced by VisionMamba (Zhu et al. 2024) and shown in Figure 4(d). A bi-directional Mamba block adapts the concept of bi-directional sequence modeling to vision-related tasks. It processes flattened visual token sequences simultaneously using forward and backward state-space models.

Our architecture consists of stacked StableMamba blocks. Within each StableMamba block are N bi-directional Mamba blocks and A Transformer blocks as shown in Figure 4(a). The purpose of the Transformer blocks is to stabilize the training and increase the robustness by resetting the focus after several bi-directional Mamba blocks more on lower frequencies. We will evaluate the impact of the number of Transformer blocks in each StableMamba block and the position of the Transformer block (within the StableMamba block) in Section 5. We now describe the two blocks in more detail.

Transformer block: The Transformer block is detailed in Figure 4(b). Each Transformer block begins with a Root Mean Square (RMS) normalization layer applied to the input data. It follows a Self-Attention layer where three learnable linear layers \mathbf{W}^Q , \mathbf{W}^K , and \mathbf{W}^V are used for transforming the input \mathbf{X} into queries (\mathbf{Q}), keys (\mathbf{K}) and values (\mathbf{V}) such that $\mathbf{Q} = \mathbf{X}\mathbf{W}^Q$, $\mathbf{K} = \mathbf{X}\mathbf{W}^K$, and $\mathbf{V} = \mathbf{X}\mathbf{W}^V$. The output \mathbf{Z} of the Self-Attention layer is then calculated as:

$$\mathbf{Z} = \text{SOFTMAX} \left(\frac{\mathbf{Q}\mathbf{K}^T}{\sqrt{D_q}} \right) \mathbf{V} \quad (3)$$

where D_q is the dimension of the query. Furthermore, a skip connection is added to the output. Subsequently, another RMS normalization is applied, after which this output is fed to an MLP layer. This constitutes the entire Transformer block shown in Figure 4(b). The operations can be summarized as:

$$\begin{aligned} \mathbf{Z}_{\text{in}} &= \text{PE} + \text{EMB}(\mathbf{X}) \\ \mathbf{Z}'_{\text{out}} &= \mathbf{Z}_{\text{in}} + \text{ATTN}(\text{RMSNORM}(\mathbf{Z}_{\text{in}})) \\ \mathbf{Z}_{\text{out}} &= \mathbf{Z}'_{\text{out}} + \text{MLP}(\text{RMSNORM}(\mathbf{Z}'_{\text{out}})) \end{aligned} \quad (4)$$

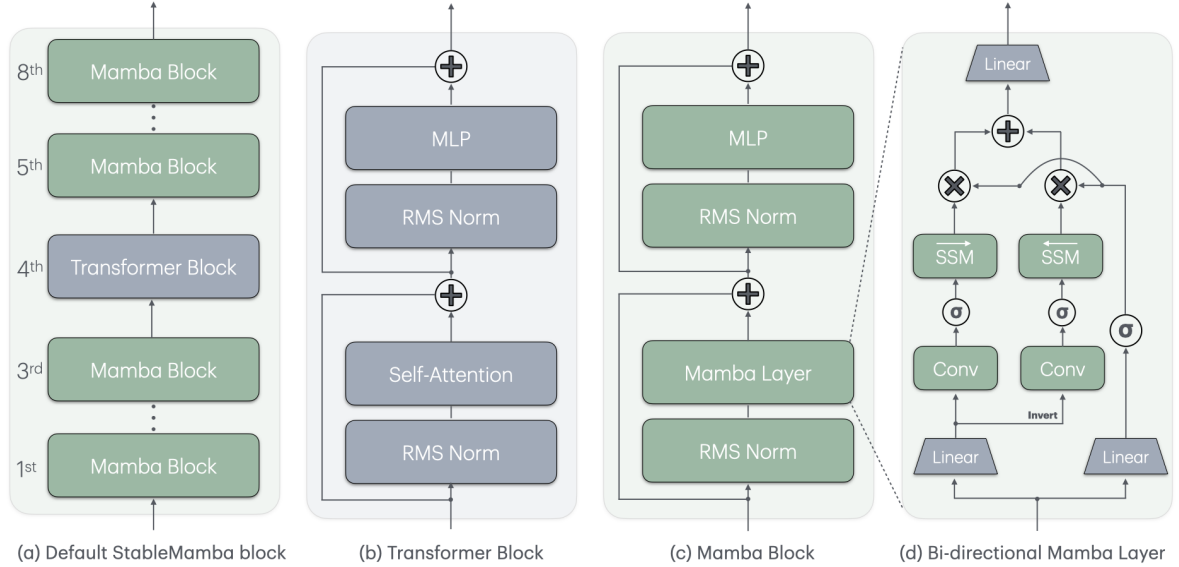


Figure 4: (a) The overall architecture of the StableMamba model. (b) Anatomy of Transformer block. (c) Anatomy of Mamba block. (d) Anatomy of bidirectional Mamba layer.

where \mathbf{X} is the input to the Transformer block. EMB is the convolutional patch embedding and PE is the positional encoding as in (Dosovitskiy et al. 2021). RMSNORM is the RMS norm layer and ATTN denotes the multi-head Self-Attention layer described in eq. (3). The MLP is defined by:

$$\text{MLP}(\text{RMSNORM}(\mathbf{Z}'_{\text{out}})) = \text{GELU}(\text{RMSNORM}(\mathbf{Z}'_{\text{out}})\mathbf{W}_1 + \mathbf{b}_1) \times \mathbf{W}_2 + \mathbf{b}_2. \quad (5)$$

Mamba block: The Mamba block (Figure 4(c)) has the same structure as the Transformer block except that it uses a bi-directional Mamba layer instead of a self-attention layer. For brevity’s sake, we will call the bi-directional Mamba layer simply as the Mamba layer. The Mamba block performs the following operations:

$$\begin{aligned} \mathbf{Z}'_{\text{out}} &= \mathbf{Z}_{\text{in}} + \text{MAMBA}(\text{RMSNORM}(\mathbf{Z}_{\text{in}})) \\ \mathbf{Z}_{\text{out}} &= \mathbf{Z}'_{\text{out}} + \text{FFN}(\text{RMSNORM}(\mathbf{Z}'_{\text{out}})). \end{aligned} \quad (6)$$

Our Mamba block differs from VideoMamba (Li et al. 2024) in that we add an RMS normalization layer and an MLP layer inside the Mamba block.

The number of parameters of the network can be controlled by the depth of the network and the embedding dimension. We introduce four variations of our model: StableMamba-Tiny has 7M parameters, StableMamba-Small has 27M parameters, StableMamba-Middle has 76M parameters, and StableMamba-Base has 101M parameters.

5 Results

We evaluate our model for image classification on ImageNet-1K (IN1K) (Deng et al. 2009) and for video

recognition on Kinetics-400 (K400) (Kay et al. 2017) and Something-Something-v2 (SSv2) (Goyal et al. 2017). For evaluating the robustness to various common corruptions, we use the ImageNet-C (IN-C) (Hendrycks and Dietterich 2019) benchmark. Note that ImageNet-C is only used for testing, but not for training.

5.1 Evaluation on ImageNet-1K

We use the IN1K (Deng et al. 2009) dataset for pre-training our models. IN1K contains 1.28M training and 50k validation images for 1000 categories. The models pre-trained on IN1K are used as an initializing point for fine-tuning on the other datasets.

Evaluation Setup: We train our models for 300 epochs, using the AdamW optimizer (Loshchilov and Hutter 2017) with a learning rate of $5e-4$, weight decay of 0.1, a batch size of 128 per GPU and input image resolution of 224 and a patch size of 16. We set the initial linear warm-up epochs as 5. We set the ratio of Transformer blocks to Mamba blocks to 1:7 for our baseline models. We use 4 nodes with 4 A100 GPUs (40GB) each for training. We do not use any automatic mixed precision. For a fair comparison, we also train our models with and without distillation to gauge the effect of distillation on the overall training scheme and architecture. The complete set of hyperparameters is provided in the supp. material.

Results: We present results for evaluating StableMamba on the IN1K dataset with other comparable methods in Table 1. We train our method with and without distillation to show the impact of distillation on the accuracy. We first compare the results without distillation. StableMamba out-

Type	Model	iso.	Image Size	#Params (M)	FLOPs (G)	IN1K Top-1%
CNN	ConvNeXt-T (Liu et al. 2022a)	✗	224 ²	29	4.5	82.1
	ConvNeXt-S (Liu et al. 2022a)	✗	224 ²	50	8.7	83.1
	ConvNeXt-B (Liu et al. 2022a)	✗	224 ²	89	15.4	83.8
CNN+SSM	VMamba-T (Liu et al. 2024b)	✗	224 ²	31	4.9	82.2
	VMamba-S (Liu et al. 2024b)	✗	224 ²	50	8.7	83.5
	VMamba-B (Liu et al. 2024b)	✗	224 ²	89	15.4	83.7
Trans.	Swin-T (Liu et al. 2021)	✗	224 ²	28	4.6	81.3
	Swin-S (Liu et al. 2021)	✗	224 ²	50	8.7	83.0
	Swin-B (Liu et al. 2021)	✗	224 ²	88	15.4	83.5
	DeiT-T (Touvron et al. 2021a)	✓	224 ²	6	1.3	72.2
	DeiT-S (Touvron et al. 2021a)	✓	224 ²	22	4.6	79.8
	DeiT-B (Touvron et al. 2021a)	✓	224 ²	87	17.6	81.8
SSM	ViM-T (Zhu et al. 2024)	✓	224 ²	7	1.1	76.1
	ViM-S (Zhu et al. 2024)	✓	224 ²	26	4.3	80.5
	VideoMamba-T (Liu et al. 2024b)	✓	224 ²	7	1.1	76.9
	VideoMamba-S (Liu et al. 2024b)	✓	224 ²	26	4.3	81.2
	VideoMamba-M (Liu et al. 2024b)	✓	224 ²	74	12.7	81.4
	VideoMamba-M [†] (Liu et al. 2024b)	✓	224 ²	74	12.7	82.8
	VideoMamba-B [†] (Liu et al. 2024b)	✓	224 ²	98	16.9	82.7
	StableMamba-T	✓	224 ²	7	1.2	77.4
	StableMamba-S	✓	224 ²	27	4.4	81.5
	StableMamba-M	✓	224 ²	76	12.9	83.1
	StableMamba-M [†]	✓	224 ²	76	12.9	83.5
	StableMamba-B	✓	224 ²	101	17.1	83.9
	StableMamba-B [†]	✓	224 ²	101	17.1	84.1

Table 1: **Performance comparison on ImageNet-1K:** We report the performance of our proposed models with state-of-the-art mamba-based models and popular convolution-based and transformer-based models on the ImageNet-1K (Deng et al. 2009) validation set. Our proposed models outperform the mamba-based models. [†] represents the results using distillation. ‘iso.’ means isotropic.

performs the current state-of-the-art isotropic visual SSM models (ViM and VideoMamba) on IN1K for all model sizes. Compared to VideoMamba, the improvement (+1.7) of StableMamba is largest for the model M, which is largest model of VideoMamba that can be trained without distillation. Note that an improvement of +1.7 on IN1K is substantial. The improvements compared to VideoMamba are visualized by the solid lines in Figure 1, which show the lack of scalability of VideoMamba. If we compare VideoMamba and StableMamba with distillation, we observe that distillation improves the accuracy for both architectures, but StableMamba still outperforms VideoMamba. The accuracy of StableMamba-B[†] is +1.4 higher than of VideoMamba-B[†]. It is interesting to note that StableMamba-B without distillation even outperforms VideoMamba-B[†] with distillation by +1.2. Most important, however, is that StableMamba can be scaled up and does not need any distillation as shown in Figure 1.

5.2 Evaluation on Video Recognition

After pre-training on IN1K, we fine-tune the models on two large-scale datasets. The first dataset, K400 (Kay et al. 2017), includes approximately 240,000 training videos and 19,000 validation videos, each about 10 seconds long, spanning 400 different human action classes. The second dataset, SSv2 (Goyal et al. 2017), consists of around 220,000 videos: 168,000 for training, 24,000 for validation, and 27,000 for testing, covering 174 different classes.

Evaluation Setup: For fine-tuning, we use a batch size of 32 for tiny and a batch size of 16 for small variants (constrained due to GPU memory limit). We set the number of

Arch.	Model	P.T.	Input Size	#Params (M)	FLOPs (G)	K400 Top-1%
CNN	SlowFast _{R101+NL} (Feichtenhofer et al. 2019)	-	80×224 ²	60	234×3×10	79.8
	X3D-M (Feichtenhofer 2020)	-	16×224 ²	4	6×3×10	76.0
	X3D-XL (Feichtenhofer 2020)	-	16×312 ²	20	194×3×10	80.4
CNN+Trans.	MViTv1-B (Fan et al. 2021)	-	32×224 ²	37	70×1×5	80.2
	MViTv2-S (Li et al. 2022b)	-	16×224 ²	35	64×1×5	81.0
	UniFormer-S (Li et al. 2022a)	IN1K	16×224 ²	21	42×1×4	80.8
	UniFormer-B (Li et al. 2022a)	IN1K	16×224 ²	50	97×1×4	82.0
	UniFormer-B (Li et al. 2022a)	IN1K	32×224 ²	50	259×3×4	83.0
Trans.	Swin-T (Liu et al. 2022b)	IN1K	32×224 ²	28	88×3×4	78.8
	Swin-B (Liu et al. 2022b)	IN1K	32×224 ²	88	88×3×4	80.6
	Swin-B (Liu et al. 2022b)	IN21K	32×224 ²	88	282×3×4	82.7
	STAM (Sharif et al. 2021)	IN21K	64×224 ²	121	1040×1×1	79.2
	TimeFormer-L (Bertasius et al. 2021)	IN21K	96×224 ²	121	2380×3×1	80.7
	ViViT-L (Arnab et al. 2021)	IN21K	16×224 ²	311	3992×3×4	81.3
Mformer-HR (Patrick et al. 2021)	Mformer-HR (Patrick et al. 2021)	IN21K	16×336 ²	311	959×3×10	81.1
	VideoMamba-T (Li et al. 2024)	IN1K	16×224 ²	7	17×3×4	78.1
SSM	VideoMamba-S (Li et al. 2024)	IN1K	16×224 ²	26	68×3×4	80.8
	VideoMamba-M [†] (Li et al. 2024)	IN1K	16×224 ²	74	202×3×4	81.9
	StableMamba-T	IN1K	16×224 ²	7	19×3×4	78.6
	StableMamba-S	IN1K	16×224 ²	27	70×3×4	81.2
	StableMamba-M	IN1K	16×224 ²	76	206×3×4	82.2
	StableMamba-M [†]	IN1K	16×224 ²	76	206×3×4	82.5

Table 2: Comparison with state-of-the-art methods on Kinetics-400 (Kay et al. 2017). [†] represents initialization with ImageNet-1K pretraining using distillation.

Arch.	Model	P.T.	#Params (M)	FLOPs (G)	SSv2 Top-1%
CNN	SlowFast _{R101} (Feichtenhofer et al. 2019)	K400	53	106×3×1	63.1
	CT-Net _{R50} (Li et al. 2020a)	IN1K	21	75×1×1	64.5
	TDN _{R50} (Wang et al. 2021)	IN1K	26	75×1×1	65.3
CNN+Trans.	MViTv1-B (Fan et al. 2021)	K400	37	71×3×1	64.7
	MViTv1-B (Fan et al. 2021)	K400	37	170×3×1	67.1
	MViTv2-S (Li et al. 2022b)	K400	35	65×3×1	68.2
	MViTv2-B (Li et al. 2022b)	K400	51	225×3×1	70.5
	UniFormer-S (Li et al. 2022a)	IN1K+K400	21	42×3×1	67.7
UniFormer-B (Li et al. 2022a)	IN1K+K400	50	97×3×1	70.4	
Trans.	Swin-B (Liu et al. 2022b)	K400	89	88×3×1	69.6
	ViViT-L (Arnab et al. 2021)	IN21K+K400	311	3992×3×4	65.4
	Mformer-HR (Patrick et al. 2021)	IN21K+K400	311	1185×3×1	68.1
	TimeFormer-HR (Bertasius et al. 2021)	IN21K	121	1703×3×1	62.5
SSM	VideoMamba-T (Li et al. 2024)	IN1K	7	9×3×2	65.1
	VideoMamba-S (Li et al. 2024)	IN1K	26	34×3×2	66.6
	VideoMamba-M [†] (Li et al. 2024)	IN1K	74	101×3×4	67.3
	StableMamba-T	IN1K	7	10×3×2	65.7
	StableMamba-S	IN1K	27	35×3×2	67.3
	StableMamba-M	IN1K	76	103×3×4	67.8
StableMamba-M [†]	IN1K	76	103×3×4	68.1	

Table 3: Comparison with state-of-the-art methods on the Something-Something-v2 (Goyal et al. 2017) dataset. [†] represents initialization with ImageNet-1K pretraining using distillation. Network input sizes are the same as mentioned in K400.

linear warm-up epochs to 5, and the total number of epochs to 70 for K400 and 35 for SSv2 as in (Li et al. 2024). We use AdamW as an optimizer and a learning rate of 4e-4. The complete list of hyperparameters for reproducibility is provided in the supp. material.

Results: StableMamba demonstrates superior performance in downstream video recognition tasks compared to VideoMamba, which is the only mamba architecture that can be applied to videos. On the K400 dataset in Table 2, StableMamba tiny and small outperform their VideoMamba counterparts without distillation. Distillation improves the accuracy for the middle models, but even with distillation StableMamba-M[†] improves the accuracy of VideoMamba-M[†] by +0.6, which is a substantial improvement on this dataset. The results on the SSv2 dataset shown in Ta-

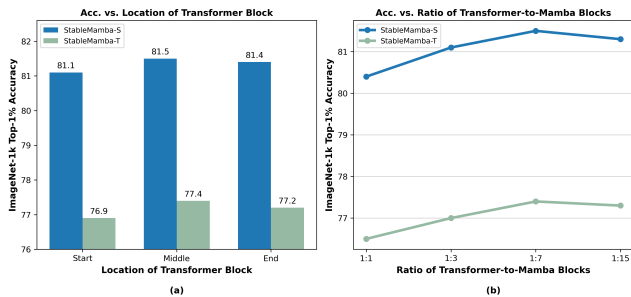


Figure 5: (a) Transformer’s position within StableMamba and its impact on performance. (b) Impact of the ratio of Transformer blocks to Mamba blocks.

ble 3 are similar, but the improvements are even larger. StableMamba-M[†] improves the accuracy of VideoMamba-M[†] by +0.8.

5.3 Evaluation on ImageNet-C

IN-C (Hendrycks and Dietterich 2019) is a benchmark for evaluating the robustness of neural networks to images with common corruptions like JPEG compression. It includes 19 common types of image corruption at 5 different intensity levels. We test our network on this benchmark to assess the robustness introduced by Attention layers.

Results: We present results for Gaussian blurring and JPEG compression corruption for StableMamba-M in comparison with VideoMamba-M, ViT-B\16 and ResNet-50 in Figure 2. We see that StableMamba-M (blue) outperforms VideoMamba-M (yellow) for all levels of corruption. The gap becomes larger as the intensity of corruption increases. StableMamba behaves similar or even slightly better than the pure attention-based architecture ViT-B\16 and is more robust than ResNet-50, in particular for the highly relevant JPEG compression setting. We report the results across all corruptions in the supplementary material.

5.4 Ablation Studies

Position of Transformer block: In Figure 4(a), the Transformer block is placed in the middle of the StableMamba blocks. This position results from our analysis of the impact on the location of the Transformer block. We conducted three experiments each for StableMamba-T and StableMamba-S, totaling six experiments, to determine the optimal position for the Transformer block. We tested placing the Transformer block at the start, middle, and end of the StableMamba blocks and evaluated their performance on the IN1K dataset. As shown in Figure 5(a), the performance of StableMamba is not highly sensitive to the Transformer’s position in both tiny and small models. However, there is a slight performance improvement when the Transformer block is in the middle. We speculate that the Transformer’s effects are most balanced in this position. Therefore, we use the middle position as the default for our StableMamba architecture.

Number of Transformer Blocks: Similar to the position of Transformer blocks within each StableMamba block, the

Model	Context Length	Training Dataset	FLOPs (G)	Accuracy
VideoMamba-T	224 ²	IN1K	1.1	76.9%
StableMamba-T	224 ²	IN1K	1.2	77.4%
VideoMamba-T	448 ²	IN1K	4.3	79.3%
StableMamba-T	448 ²	IN1K	4.5	79.9%
VideoMamba-T	16 × 224 ²	K400	17 × 3 × 4	78.1%
StableMamba-T	16 × 224 ²	K400	19 × 3 × 4	78.6%
VideoMamba-T	32 × 224 ²	K400	34 × 3 × 4	78.8%
StableMamba-T	32 × 224 ²	K400	37 × 3 × 4	79.3%

Table 4: Long-context performance comparison of StableMamba and other SSM-based models.

ratio of Transformer blocks to Mamba blocks is another design parameter for the StableMamba block. We interleave a Transformer block for every k Mamba block; for example, we interleave one Transformer block for every seven Mamba blocks. To evaluate the impact of the ratio, we conducted experiments varying the number of Mamba blocks per Transformer block. As shown in Figure 5(b), the performance on the IN1K dataset improves as the number of Mamba blocks per Transformer block increases, reaching optimal accuracy at a ratio of 1:7. Beyond this ratio, the performance decreases. Therefore, we set the design parameter to one Transformer block for every seven Mamba blocks in the StableMamba architecture.

Dependence on context length: Apart from the network architecture itself, it is interesting to investigate the network with context lengths of different sizes. To probe the suitability of our approach for a long context, we perform additional experiments. First, we train StableMamba-T with a longer context for video classification, using 32 frames instead of the usual 16 frames. Second, we train StableMamba with a larger resolution (448 instead of 224) to see its effect on image classification as well. The results in Table 4 show that StableMamba and VideoMamba benefit from the increased context length, which is a general strength of mamba-based architectures. In all cases, StableMamba outperforms VideoMamba.

6 Conclusion

We have investigated and addressed the scalability challenge in large visual state-space models by proposing a straightforward interleaved design that scales effectively to a substantial number of parameters, consistently outperforming smaller models. Our ablation studies provide insights regarding optimal positioning, the number of attention layers in the architecture, and its robustness to common corruptions in the input like JPEG compression. Extensive experiments show that our method enables the scaling of Mamba-based models to over 100M parameters, significantly enhancing performance while also improving overall robustness. Evaluations on the K400 and SSv2 datasets for video recognition validate that our approach achieves state-of-the-art results.

References

Arnab, A.; Dehghani, M.; Heigold, G.; Sun, C.; Lučić, M.; and Schmid, C. 2021. Vivit: A video vision transformer. In

ICCV.

Bertasius, G.; Wang, H.; and Torresani, L. 2021. Is space-time attention all you need for video understanding? In *ICML*.

Carreira, J.; and Zisserman, A. 2017. Quo vadis, action recognition? a new model and the kinetics dataset. In *CVPR*.

Chen, G.; Huang, Y.; Xu, J.; Pei, B.; Chen, Z.; Li, Z.; Wang, J.; Li, K.; Lu, T.; and Wang, L. 2024. Video Mamba Suite: State Space Model as a Versatile Alternative for Video Understanding. *arxiv preprint, arXiv:2403.09626*.

Dao, T. 2023. Flashattention-2: Faster attention with better parallelism and work partitioning. *arXiv preprint, arXiv:2307.08691*.

Dao, T.; Fu, D.; Ermon, S.; Rudra, A.; and Ré, C. 2022. Flashattention: Fast and memory-efficient exact attention with io-awareness. *NeurIPS*.

Deng, J.; Dong, W.; Socher, R.; Li, L.-J.; Li, K.; and Fei-Fei, L. 2009. ImageNet: A large-scale hierarchical image database. In *CVPR*.

Dosovitskiy, A.; Beyer, L.; Kolesnikov, A.; et al. 2021. An Image is Worth 16x16 Words: Transformers for Image Recognition at Scale. In *ICLR*.

Duan, H.; Zhao, Y.; Xiong, Y.; Liu, W.; and Lin, D. 2020. Omni-sourced webly-supervised learning for video recognition. In *ECCV*.

Fan, H.; Xiong, B.; Mangalam, K.; Li, Y.; Yan, Z.; Malik, J.; and Feichtenhofer, C. 2021. Multiscale vision transformers. In *ICCV*.

Feichtenhofer, C. 2020. X3D: Expanding Architectures for Efficient Video Recognition. In *CVPR*.

Feichtenhofer, C.; Fan, H.; Malik, J.; and He, K. 2019. Slow-fast networks for video recognition. In *ICCV*.

Feichtenhofer, C.; Pinz, A.; and Wildes, R. 2016. Spatiotemporal Residual Networks for Video Action Recognition. In *NeurIPS*.

Fu, D. Y.; Dao, T.; Saab, K. K.; Thomas, A. W.; Rudra, A.; and Ré, C. 2023. Hungry hungry hippos: Towards language modeling with state space models. In *ICLR*.

Gong, H.; Kang, L.; Wang, Y.; Wan, X.; and Li, H. 2024. nmmamba: 3d biomedical image segmentation, classification and landmark detection with state space model. *arxiv preprint, arXiv:2402.03526*.

Gou, J.; Yu, B.; Maybank, S. J.; and Tao, D. 2020. Knowledge Distillation: A Survey. *IJCV*.

Goyal, R.; Ebrahimi Kahou, S.; Michalski, V.; et al. 2017. The "something something" video database for learning and evaluating visual common sense. In *ICCV*.

Gu, A.; and Dao, T. 2023. Mamba: Linear-time sequence modeling with selective state spaces. *arxiv preprint, arXiv:2312.00752*.

Gu, A.; Goel, K.; and Ré, C. 2022. Efficiently modeling long sequences with structured state spaces. In *ICLR*.

Guo, H.; Li, J.; Dai, T.; Ouyang, Z.; Ren, X.; and Xia, S.-T. 2024. MambaR: A Simple Baseline for Image Restoration with State-Space Model. *arxiv preprint, arXiv:2402.15648*.

Guo, T.; Wang, Y.; and Meng, C. 2024. Mambamorph: a mamba-based backbone with contrastive feature learning for deformable mr-ct registration. *arxiv preprint, arXiv:2401.13934*.

He, K.; Zhang, X.; Ren, S.; and Sun, J. 2016. Deep Residual Learning for Image Recognition. In *CVPR*.

He, X.; Cao, K.; Yan, K.; Li, R.; Xie, C.; Zhang, J.; and Zhou, M. 2024. Pan-Mamba: Effective pan-sharpening with State Space Model. *arxiv preprint, arXiv:2402.12192*.

Hendrycks, D.; and Dietterich, T. 2019. Benchmarking neural network robustness to common corruptions and perturbations. *arXiv preprint, arXiv:1903.12261*.

Howard, A. G.; and Bo Chen, M. Z.; Kalenichenko, D.; Wang, W.; Weyand, T.; Andreetto, M.; and Adam, H. 2017. MobileNets: Efficient Convolutional Neural Networks for Mobile Vision Applications. *arxiv preprint, arXiv:1704.04861*.

Huang, T.; Pei, X.; You, S.; Wang, F.; Qian, C.; and Xu, C. 2024. LocalMamba: Visual State Space Model with Windowed Selective Scan. *arxiv preprint, arXiv:2403.09338*.

Karpathy, A.; Toderici, G.; Shetty, S.; Leung, T.; Sukthankar, R.; and Fei-Fei, L. 2014. Large-scale video classification with convolutional neural networks. In *CVPR*.

Kay, W.; Carreira, J.; Simonyan, K.; Zhang, B.; Hillier, C.; Vijayanarasimhan, S.; Viola, F.; Green, T.; Back, T.; Natsev, P.; et al. 2017. The kinetics human action video dataset. *arXiv preprint, arXiv:1705.06950*.

Klaser, A.; Marszałek, M.; and Schmid, C. 2008. A spatio-temporal descriptor based on 3d-gradients. In *BMVC*.

Kondratyuk, D.; Yuan, L.; Li, Y.; Zhang, L.; Tan, M.; Brown, M.; and Gong, B. 2021. Movinets: Mobile video networks for efficient video recognition. In *CVPR*.

Krizhevsky, A.; Sutskever, I.; and Hinton, G. E. 2012. ImageNet Classification with Deep Convolutional Neural Networks. In *NeurIPS*.

Laptev, and Lindeberg. 2003. Space-time interest points. In *ICCV*.

Li, K.; Li, X.; Wang, Y.; He, Y.; Wang, Y.; Wang, L.; and Qiao, Y. 2024. VideoMamba: State Space Model for Efficient Video Understanding. *arxiv preprint, arXiv:2403.06977*.

Li, K.; Li, X.; Wang, Y.; Wang, J.; and Qiao, Y. 2020a. CT-Net: Channel Tensorization Network for Video Classification. In *ICLR*.

Li, K.; Wang, Y.; Gao, P.; Song, G.; Liu, Y.; Li, H.; and Qiao, Y. 2022a. UniFormer: Unified Transformer for Efficient Spatiotemporal Representation Learning. In *ICLR*.

Li, Y.; Ji, B.; Shi, X.; Zhang, J.; Kang, B.; and Wang, L. 2020b. TEA: Temporal Excitation and Aggregation for Action Recognition. In *CVPR*.

Li, Y.; Wu, C.-Y.; Fan, H.; Mangalam, K.; Xiong, B.; Malik, J.; and Feichtenhofer, C. 2022b. MVITv2: Improved multi-scale vision transformers for classification and detection. In *CVPR*.

- Liang, D.; Zhou, X.; Wang, X.; Zhu, X.; Xu, W.; Zou, Z.; Ye, X.; and Bai, X. 2024. PointMamba: A Simple State Space Model for Point Cloud Analysis. *arxiv preprint, arXiv:2402.10739*.
- Lin, J.; Gan, C.; and Han, S. 2019. Tsm: Temporal shift module for efficient video understanding. In *ICCV*.
- Liu, J.; Yang, H.; Zhou, H.-Y.; Xi, Y.; Yu, L.; Yu, Y.; Liang, Y.; Shi, G.; Zhang, S.; Zheng, H.; et al. 2024a. Swinmamba: Mamba-based unet with imagenet-based pretraining. *arxiv preprint, arXiv:2402.03302*.
- Liu, Y.; Tian, Y.; Zhao, Y.; Yu, H.; Xie, L.; Wang, Y.; Ye, Q.; and Liu, Y. 2024b. VMamba: Visual State Space Model. *arxiv preprint, arXiv:2401.10166*.
- Liu, Z.; Lin, Y.; Cao, Y.; Hu, H.; Wei, Y.; Zhang, Z.; Lin, S.; and Guo, B. 2021. Swin Transformer: Hierarchical Vision Transformer using Shifted Windows. In *ICCV*.
- Liu, Z.; Mao, H.; Wu, C.-Y.; Feichtenhofer, C.; Darrell, T.; and Xie, S. 2022a. A convnet for the 2020s. In *CVPR*.
- Liu, Z.; Ning, J.; Cao, Y.; Wei, Y.; Zhang, Z.; Lin, S.; and Hu, H. 2022b. Video Swin Transformer. In *CVPR*.
- Liu, Z.; et al. 2022c. Swin Transformer V2: Scaling Up Capacity and Resolution. In *CVPR*.
- Loshchilov, I.; and Hutter, F. 2017. Fixing Weight Decay Regularization in Adam. *arxiv preprint, arXiv:1711.05101*.
- Ma, J.; Li, F.; and Wang, B. 2024. U-mamba: Enhancing long-range dependency for biomedical image segmentation. *arxiv preprint, arXiv:2401.04722*.
- Mehta, H.; Gupta, A.; Cutkosky, A.; and Neyshabur, B. 2022. Long range language modeling via gated state spaces. *arxiv preprint, arXiv:2206.13947*.
- Naseer, M. M.; Ranasinghe, K.; Khan, S. H.; Hayat, M.; Shahbaz Khan, F.; and Yang, M.-H. 2021. Intriguing properties of vision transformers. In *NeurIPS*.
- Ng, J. Y.-H.; Hausknecht, M.; Vijayanarasimhan, S.; Vinyals, O.; Monga, R.; and Toderici, G. 2015. Beyond Short Snippets: Deep Networks for Video Classification. In *CVPR*.
- Patrick, M.; Campbell, D.; Asano, Y.; Misra, I.; Metze, F.; Feichtenhofer, C.; Vedaldi, A.; and Henriques, J. F. 2021. Keeping your eye on the ball: Trajectory attention in video transformers. In *NeurIPS*.
- Patro, B. N.; and Agneeswaran, V. S. 2024. SiMBA: Simplified Mamba-Based Architecture for Vision and Multivariate Time series. *arxiv preprint, arXiv:2403.15360*.
- Pei, X.; Huang, T.; and Xu, C. 2024. EfficientVMamba: Atrous Selective Scan for Light Weight Visual Mamba. *arxiv preprint, arXiv:2403.09977*.
- Qiu, Z.; Yao, T.; Ngo, C.-W.; Tian, X.; and Mei, T. 2019. Learning Spatio-Temporal Representation With Local and Global Diffusion. In *CVPR*.
- Ruan, J.; and Xiang, S. 2024. Vm-unet: Vision mamba unit for medical image segmentation. *arxiv preprint, arXiv:*
- Sharir, G.; Noy, A.; and Zelnik-Manor, L. 2021. An Image is Worth 16x16 Words, What is a Video Worth? *arxiv preprint, arxiv:2103.13915*.
- Simonyan, K.; and Zisserman, A. 2014. Two-stream convolutional networks for action recognition in videos. In *NeurIPS*.
- Simonyan, K.; and Zisserman, A. 2015. Very Deep Convolutional Networks for Large-Scale Image Recognition. *ICLR*.
- Smith, J. T.; Warrington, A.; and Linderman, S. W. 2023. Simplified state space layers for sequence modeling. In *ICLR*.
- Sun, L.; Jia, K.; Yeung, D.-Y.; and Shi, B. E. 2015. Human action recognition using factorized spatio-temporal convolutional networks. In *ICCV*.
- Szegedy, C.; Liu, W.; Jia, Y.; Sermanet, P.; Reed, S.; Anguelov, D.; Erhan, D.; Vanhoucke, V.; and Rabinovich, A. 2015. Going deeper with convolutions. In *CVPR*.
- Szegedy, C.; Vanhoucke, V.; Ioffe, S.; Shlens, J.; and Wojna, Z. 2016. Rethinking the inception architecture for computer vision. In *CVPR*.
- Tan, M.; and Le, Q. V. 2019. EfficientNet: Rethinking Model Scaling for Convolutional Neural Networks. In *ICML*.
- Touvron, H.; Cord, M.; Douze, M.; Massa, F.; Sablayrolles, A.; and Jegou, H. 2021a. Training data-efficient image transformers & distillation through attention. In *ICML*.
- Touvron, H.; Cord, M.; Sablayrolles, A.; Synnaeve, G.; and Jégou, H. 2021b. Going deeper with image transformers. In *ICCV*.
- Tran, D.; Bourdev, L.; Fergus, R.; Torresani, L.; and Paluri, M. 2015. Learning spatiotemporal features with 3d convolutional networks. In *ICCV*.
- Tran, D.; Wang, H.; Torresani, L.; Ray, J.; LeCun, Y.; and Paluri, M. 2018. A closer look at spatiotemporal convolutions for action recognition. In *CVPR*.
- Vaswani, A.; Shazeer, N.; Parmar, N.; Uszkoreit, J.; Jones, L.; Gomez, A. N.; Kaiser, Ł.; and Polosukhin, I. 2017. Attention is all you need. In *NeurIPS*.
- Wang, C.; Tsepa, O.; Ma, J.; and Wang, B. 2024. Graph-Mamba: Towards Long-Range Graph Sequence Modeling with Selective State Spaces. *arxiv preprint, arXiv:2402.00789*.
- Wang, H.; Kläser, A.; Schmid, C.; and Liu, C.-L. 2013. Dense trajectories and motion boundary descriptors for action recognition. *IJCV*.
- Wang, H.; Wu, X.; Huang, Z.; and Xing, E. P. 2020a. High-frequency component helps explain the generalization of convolutional neural networks. In *CVPR*.
- Wang, L.; Tong, Z.; Ji, B.; and Wu, G. 2021. TDN: Temporal difference networks for efficient action recognition. In *CVPR*.
- Wang, X.; Girshick, R.; Gupta, A.; and He, K. 2018. Non-local Neural Networks. In *CVPR*.
- Wang, X.; Xiong, X.; Neumann, M.; Piergiovanni, A.; Ryoo, M. S.; Angelova, A.; Kitani, K. M.; and Hua, W. 2020b. Attentionnas: Spatiotemporal attention cell search for video classification. In *ECCV*.

Wasim, S. T.; Khattak, M. U.; Naseer, M.; Khan, S.; Shah, M.; and Khan, F. S. 2023. Video-FocalNets: Spatio-Temporal Focal Modulation for Video Action Recognition. In *ICCV*.

Woo, S.; Debnath, S.; Hu, R.; Chen, X.; Liu, Z.; Kweon, I. S.; and Xie, S. 2023. ConvNeXt V2: Co-designing and Scaling ConvNets with Masked Autoencoders. In *CVPR*.

Xiao, T.; Singh, M.; Mintun, E.; Darrell, T.; Dollár, P.; and Girshick, R. 2021. Early convolutions help transformers see better. In *NeurIPS*.

Xie, S.; Sun, C.; Huang, J.; Tu, Z.; and Murphy, K. 2018. Rethinking spatiotemporal feature learning: Speed-accuracy trade-offs in video classification. In *ECCV*.

Yan, S.; Xiong, X.; Arnab, A.; Lu, Z.; Zhang, M.; Sun, C.; and Schmid, C. 2022. Multiview Transformers for Video Recognition. In *CVPR*.

Yang, J.; Li, C.; Dai, X.; Yuan, L.; and Gao, J. 2022. Focal Modulation Networks. In *NeurIPS*.

Yang, Y.; Xing, Z.; and Zhu, L. 2024. Vivim: a video vision mamba for medical video object segmentation. *arxiv preprint, arXiv:2401.14168*.

Zhang, Y.; Li, X.; Liu, C.; Shuai, B.; Zhu, Y.; Brattoli, B.; Chen, H.; Marsic, I.; and Tighe, J. 2021. Vidtr: Video transformer without convolutions. In *ICCV*.

Zhu, L.; Liao, B.; Zhang, Q.; Wang, X.; Liu, W.; and Wang, X. 2024. Vision Mamba: Efficient Visual Representation Learning with Bidirectional State Space Model. *arxiv preprint, arXiv:2401.09417*.